# A Regional-Scale Particle-Tracking Method for Nonstationary Fractured Media

Johan Öhman[1], Auli Niemi[1] and Chin-Fu Tsang[2]

[1]Air and Water Science, Department of Earth Sciences, Uppsala University, Sweden
[2] Earth Sciences Division, Ernest Orlando Lawrence Berkeley National Laboratory, US

**Abstract.** A regional scale transport model is introduced that is applicable to non-stationary and statistically inhomogeneous fractured media, provided that hydraulic flow, but not necessarily solute transport, can be approximated by equivalent continuum properties at some block scale. Upscaled flow and transport block properties are transferred from multiple fracture network realizations to a regional model with grid elements of equal size to that found valid for continuum approximation of flow. In the large-scale model, flow is solved in a stochastic continuum framework, whereas the transport calculations employ a random walk procedure. Block-wise transit times are sampled from distributions linked to each block-conductivity based on its underlying fracture network. To account for channeled transport larger than the block scale, several alternatives in sampling algorithm are introduced and compared. The most reasonable alternative incorporates a spatial persistence length in sampling the particle transit times; this tracer transport persistence length is related to interblock channeling, and is quantified by the number $N$ of blocks. The approach is demonstrated for a set of field data, and the obtained regional-scale particle breakthroughs are analyzed. These are fitted to the one-dimensional advective-dispersive equation to determine an effective macroscale dispersion coefficient. An interesting finding is that this macroscale dispersion coefficient is found to be a linear function of the transport persistence, $N$, with a slope equal to a representative mean block-scale dispersion coefficient and a constant that incorporates background dispersion arising from the regional heterogeneous conductivity field.

## 1. Introduction

Modeling flow and transport in fractured rock is complicated by strong heterogeneity, which makes predictions of tracer transport from local observations and their upscaling for large-scale models a challenging task. However, use of local small-scale data is necessary; because of the low conductivity and consequently slow response, very few large-scale tracer transport experiments have been conducted in fractured media. *Tsang and Neretnieks* (1998) reviewed available field experiments and analysis methods. More recently, tracer experiments for transport characterization in fracture media have been carried out at small scale (e.g., *Sidle et al.*, 1998), intermediate scale (*Kosakowski*, 2004) and kilometer scale [*Becker and Shapiro* (2000); *Shapiro* (2001)]. As pointed out by *Tsang and Neretnieks* (1998) the tracer breakthrough curves typically display anomalous breakthrough curves, characterized by early initial arrival and extraordinarily long tails that exhibit a slow decay. Fitting breakthrough curves to the analytical one-dimensional advection-dispersion equation (ADE), indicates that this tailing may result from variable advective velocity among different flow paths [*Kosakowski* (2004); *Becker and Shapiro* (2000); *Shapiro* (2001); see also *Tsang and Tsang* (1987) and *Moreno and Tsang* (1994)] and/or diffusive mass transfer between flow paths and either stagnant water or an essentially infinite rock matrix [*Cvetkovic* (1999); *Andersson et al.* (2004)].

In terms of modeling, three basic approaches have been adopted: (a) the deterministic equivalent porous medium approach, (b) the stochastic continuum approach, and (c) the fracture network approach. The range of applicability of these alternative approaches depends on the scale of the heterogeneity in relation to the scale of the region of interest. The deterministic-porous medium approach is applicable to the largest of scales, and the fracture network approach to the smallest of scales, where flow and transport in individual fractures may be important. The applicability range of the stochastic continuum approach falls in between these cases, i.e., for scales where the heterogeneity effects are of interest but can be represented by means of stochastic continuum properties. A more detailed review of different approaches for modeling flow in fractured media is given in *Öhman and Niemi* (2003). Several recent works also employ some hybrid approach where fracture network models are used to derive input for stochastic continuum models. In such cases, the scale at which the continuum approximation can be adopted must be properly determined.

It has been demonstrated in various experiments (e.g., *Neretnieks*, 1993) that in fractured rock, the distribution of transport pathways can be very different from those of flow patterns. Therefore transport does not necessarily exhibit continuum behavior at the same support scale for which continuum conductivity tensors can be determined for flow (*Endo et al*., 1984). Furthermore, even if an effective transport property can be determined at some meaningful support scale to justify the use of a stochastic continuum analysis for transport, the finite difference and finite-element solutions of the ADE in strongly heterogeneous conductivity fields can show severe numerical dispersion (e.g., *Hoffman*, 2001).

Because of the difficulties in applying continuum models for transport, on the one hand, and the limits of applicability of fracture network models, on the other, innovative new methods are needed to solve regional scale problems [*NRC* (1996); *Berkowitz* (2002)]. Many of the recent approaches rely on various forms of stochastic Lagrangian methods [e.g., *Shulan et al*. (2001); *Bruderer and Bernabe* (2001); *Cvetkovic et al*. (2004)]. Typically, a combination of particle tracking and random walk is used (e.g., *Scher et al*., 2002). In their pioneering work, *Schwartz and Smith* (1988) introduced a hybrid method to upscale fracture network-based transport to be used as input for a large-scale equivalent-porous-medium model and owing to its feasibility, their approach is still being used [e.g., *Abbo et al.* (2003); *Carneiro* (2003)]. In this approach, stochastic particle motion is learnt from particle tracking in a "subdomain" fracture network, which is exposed to a gradually rotated hydraulic gradient. Assuming statistical homogeneity, fitted particle-motion distributions are then sampled in a random walk through a regional-scale head-field, which is solved by deterministic continuum modeling. The approach was later improved by accounting for preferential flow (*Parney and Smith*, 1995), i.e., including correlation between particle velocity and path length that is also determined from the "subdomain." Recently, the linear Boltzmann transport equation was used in a rather similar hybrid approach to describe particle motion in fractured media (*Benke and Painter*, 2003). Fracture intersections are represented by "molecule collisions" in a fluid, in the sense that they may cause abrupt changes in the direction and velocity of a particle under a random walk. Preferential flow is accounted for by fracture-intersection-transition probabilities, which are obtained from particle tracking in small fracture networks.

In spite of the great progress made during the last twenty years in characterizing and describing flow and transport in fractured media, models for field-scale transport are still preliminary in character in terms of their capability to take site-specific heterogeneity into account. The present work introduces a new approach for this purpose. We start from the detailed-scale geological and hydraulic data and employ fracture network modeling to obtain the relevant flow and transport statistics at some support scale, for which flow, but not necessarily transport, can be represented by means of a continuum. We then use stochastic continuum flow simulation in combination with large scale particle tracking to model transport. Here, particle velocities determined from the network realizations are transferred to a large-scale model via a specific scaling method. Special attention is given to transport channeling characteristics; this is modeled by a superimposed "tracer transport persistence," $N$, in our sampling algorithm. Furthermore, to show the feasibility of allowing for realistic field conditions, a depth trend in flow and transport characteristics, caused by the closing of fractures with increasing stress, is also included.

In the following, we will first present the approach, and then apply it to a set of field data, to study a hypothetical scenario related to deep disposal of high-level nuclear waste. We use data from Sellafield, England, as an example (*Andersson and Knight*, 2000). Sellafield is a fractured rock site that has been intensively investigated by Nirex (e.g., *Nirex*, 1997a-d) in connection with nuclear waste disposal. The database we use is not complete and is not intended to reflect the characteristics of the site in general, but is taken merely as an example of a realistic fractured rock database to demonstrate our method.

## 2. Model for Regional-Scale Transport in Fractured Media

### 2.1 Overview of the Model

Our objective is to introduce a model for large-scale solute transport in fracture media that properly honors the fracture-related heterogeneity observed in boreholes via a fracture network-based upscaling. The suggested approach is inspired by *Nordqvist et al.* (1992), who transferred statistics of within-fracture plane channeled transport, evoked by variable aperture, onto a flow field solved for a constant-aperture fracture network. In their approach, transit time distributions are first determined by particle tracking in individual

fracture planes with variable aperture. Transport is then modeled by a random walk through a three-dimensional fracture network (*Dverstorp and Andersson*, 1989), where at each fracture the previously obtained distributions are sampled, with appropriate rescaling for local gradients (*Tsang*, 1993). In this paper, we seek to utilize their innovative concept, but at a larger scale, as explained below.

The three different scales being addressed here are: regional scale, block scale, and detailed scale. We define the regional scale by a kilometer-scale domain for which transport is ultimately to be solved. The block scale is defined by a cubic domain with side-length 7.5 m, for which it has been found that flow in fracture networks can be represented by conductivity tensors of equivalent porous media (i.e., it is the scale for a "continuum approximation" of hydraulic flow). The 7.5 m value is based on a study of the current data set (*Öhman and Niemi*, 2003). The detailed scale refers to fracture network geometry and individual fractures that govern the transport properties of the medium (and in particular of the blocks). Our approach relies on a "hybrid" concept, that the detailed fracture-scale properties are transferred via the block scale at the regional scale; it can briefly be summarized as follows:

1. The hydraulic characteristics of a large number of fracture network realizations are studied to determine continuum tensors for hydraulic conductivity at the block scale that are then used as a support scale (*Neuman*, 1987) for a regional-scale stochastic continuum model.

2. Tracer-transport behavior is learned from the same block-scale fracture network realizations as were used to determine the continuum conductivity tensors. A large number of particles are released, and their mean transport velocities within a fracture network block are collected as a probability distribution. It can be expected (as demonstrated later) that transport does not exhibit continuum characteristics at the block scale and, hence, an equivalent dispersion tensor approach cannot be used. Consequently, distributions of particle transit times at block scale will be used directly in the subsequent regional-scale simulations.

3. Regional-scale flow fields are simulated with a stochastic continuum model. This model is discretized to the block scale, and the distribution of upscaled conductivity, determined in step 1, is used as input.

4. Regional-scale transport is modeled in terms of particle steps by sampling from the previously obtained block-scale transit times. Each upscaled block conductivity value is linked to its own transit time distribution, since steps 1 and 2 are conducted for the same network realizations, representing the same block. Special emphasis is given to how this sampling is done, as will be discussed in more detail later. Furthermore, to obtain the proper transit time at each step in the regional-scale model, the sampled transit times need to be scaled according to the local ambient hydraulic gradient.

The software used for the fracture network modeling includes FracMan (*Dershowitz et al.,* 1998) for generating the complex fracture network geometries, and MAFIC (*Miller et al.,* 1999) for solving the flow equations and particle transport in these networks. The regional-scale stochastic continuum modeling is done with TOUGH (*Pruess et al.,* 1999), an integral finite difference-based model, which is further developed to include the present transport analysis. In the following sections, the various steps are described in more detail.

### 2.2 Upscaling Fracture Network Properties at Block Scale

#### 2.2.1 Block-Scale Hydraulic Conductivity

For upscaling hydraulic conductivities, we use the classical upscaling of fractured media, originally introduced by *Long et al.* (1982), and later implemented by, for example, *Cacas et al.* (1990). This analysis was carried out for the present data and its detail is described by *Öhman and Niemi* (2003); hence, only the main points will be repeated here. In this approach, an imposed hydraulic gradient is gradually rotated with respect to the fracture network to determine the equivalent conductivity $K$ in each direction. If the shape of this conductivity (as $1/\sqrt{(K)}$) versus rotational angle resembles a smooth ellipse, its conductivity can be represented by means of a continuum conductivity tensor. In this earlier study, a block size of 7.5 m was found that allowed such a continuum representation, i.e., most of the fracture network realizations followed continuum behavior sufficiently well.

Flow is simulated at this block scale for multiple stochastic realizations to determine distributions of continuum conductivity tensors. Only the horizontal and vertical components of conductivity are used below as input for generating stochastic continuum realizations for the two-dimensional finite difference-based regional-scale model.

The hydraulic conductivity of fractured rock is known to decrease with increasing depth, due to fracture closure with increasing stress. This depth trend is incorporated into the model, based on a hydromechanical coupling described in detail by *Öhman et al.* (2004). In principle, this approach accounts for fracture closure by using a stress-aperture closure relationship measured in the laboratory. In the present work, the rock is divided into four different depth intervals for which the principal stresses are known, and different statistical distributions of equivalent conductivity are then obtained for each depth interval to correspond to the different stress levels.

### 2.2.2 Block-Scale Transport Properties

Particle transport is then studied at the block scale, at which the continuum representation of flow is valid. It would have been convenient, if an equivalent continuum dispersivity could be found in a similar way and at the same scale. This is studied by analyzing particle breakthrough as a function of rotational angle. As will be shown later, the results indicate that a dispersion tensor representation is not valid for the block scale selected. Therefore another approach is used to transfer block-scale particle transit times, $\tau$, to the regional-scale stochastic continuum model. The transit time is defined as

$$\tau(s) = \int_0^s \frac{ds}{v(s)} \tag{1}$$

where $v$ is the spatially varying fluid velocity along the trajectory at a distance $s$ from release point.

To obtain particle transit times for each fracture network realization $i$ at the block scale, a large number of particles, typically 10,000, are released and their transit time distributions $g_i(\tau_p)$ are determined, where $p$ refers to particle number. Because of the structure

of the numerical simulator used in the regional-scale model, transit time statistics is needed separately for the "upstream" and "downstream" sections of a fracture-network block. The reason for this is that to attain consistency in the configuration of boundary conditions for the integral finite difference model and for the fracture network model, particles must move from one nodal point to another in the regional-scale model; and, as explained in section 2.3.2, these nodal points are located at the center of numerical elements. Therefore transit times are determined separately for the "upstream section" (i.e., from the boundary with higher hydraulic head to the center of the block) and for the "downstream section" (i.e., from the center of the block to the boundary with lower hydraulic head) and are denoted as ${}^{A}\tau$ and ${}^{B}\tau$, respectively. This is visualized in Figure 1.

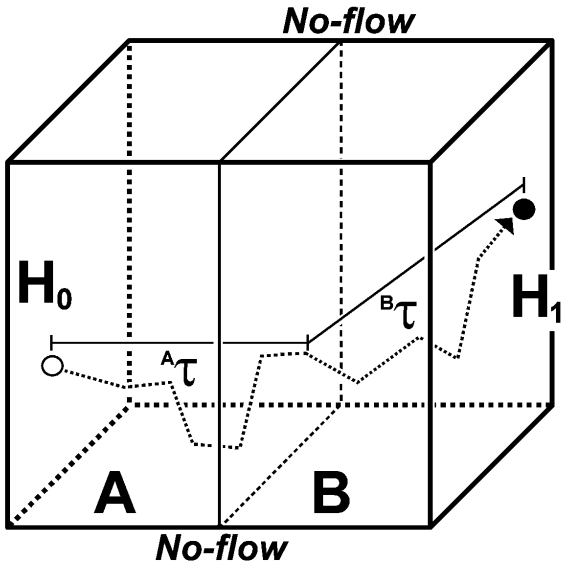


**Figure 1.** Geometry and boundary conditions of the block-scale particle-tracking domain, divided into two halves, an "upstream" section *A* and a "downstream" section *B*, with imposed constant head boundary conditions $H_0 > H_1$.

Also, we carry out the particle-tracking procedure for networks corresponding to the four different depth intervals, adjusted to the four different stress-levels.

The results are organized to enable a correct linking between block-scale transport properties and block conductivities in the following regional-scale simulations. In other words, for each network realization, *i*, we save the vertical and horizontal components of conductivity, $K_{iv}$ and $K_{ih}$, and four distributions of transit times, $g_{iv}({}^{A}\tau_p)$, $g_{iv}({}^{B}\tau_p)$, $g_{ih}({}^{A}\tau_p)$ and

$g_{ih}({}^{B}\tau_p)$ and denote them with the same index $i$. Also, the calculated transit times in each distribution are ranked in ascending order, from shortest transit time to longest, and given a rank $m$ that varies from 1 to the total number of particles released (the smallest value of $m$ corresponds to the fastest pathway and the largest $m$ to the slowest pathway through the block element). The reason for saving this information is that we shall use it to carry pathway information between block elements in the regional-scale particle-tracking model, as will be explained later in section 2.3.3. When this ranking $m$ is discussed, we use the notation $g_i({}^{A}\tau_m)$ and $g_i({}^{B}\tau_m)$.

## 2.3 Regional-Scale Stochastic continuum Model

### 2.3.1 Stochastic Flow Model

Multiple stochastic continuum realizations of regional-scale flow fields are generated based on conductivity distributions at the block scale (section 2.2.1). Correlated conductivity fields for the regional scale are calculated using the GSLIB software (*Deutsch and Journel*, 1998). Each block element in the regional model has a conductivity value $K_i$ and is linked to its corresponding particle transit time distribution is then $g_i(\tau)$. For the regional-scale flow modeling, we use the numerical simulator TOUGH2 (*Pruess et al.,* 1999), which employs an integral finite difference method for the numerical flow solution. In this numerical method, property values are calculated at nodal points located at the center of elements. This poses an additional complication when importing the upscaled values to the regional-scale model, because the transport between two nodal points actually involves properties of two block elements.

### 2.3.2 Rules of Particle Movement

The particle transport in these regional-scale stochastic continuum realizations is then modeled by first solving the flow fields, releasing a large number of particles (we used $10^6$) and then observing their transport. The particle movement is simulated according to the following:

1. A particle moves from its present block element, in direction $k$, to an adjacent element with probability, $P_k$, which is proportional to the total outward directed flux in that direction, $Q_k^{out}$, as defined by

$$P_k = \frac{Q_k^{out}}{\sum_k Q_k^{out}} \tag{2}$$

where $\sum_k Q_k^{out}$ is the sum of all fluxes out of the element. This is visualized in Figure 2a.

2. The particle first moves from the node situated at the center of the present block element, through section $B$ of the that element, crosses the element interface and moves through section $A$ of an adjacent element, until reaching the neighboring element node, as shown in Figure 2b. Transport times for both sections (sections $B$ and $A'$) are sampled from the block-specific transit time distributions, $g_i({}^{B}\tau_m)$ and $g_{i'}({}^{A'}\tau_m)$, associated with each element. The prescription for sampling of distributions is discussed separately in section 2.3.3.

3. Particle transport in the regional-scale model is subject to the local ambient hydraulic gradient ($\Delta H_{amb}/\Delta x_{amb}$) across the block element and the transit times from $g_i(\tau_m)$ are rescaled for this local hydraulic gradient. Based on the well-known relationship between velocity and transit time, as well as expressions for linear flow velocity, the scaling for a fixed distance is determined from

$$\tau_{amb} = \frac{K_{netw}/\phi_{netw}}{K_{amb}/\phi_{amb}} \frac{\Delta H_{netw}/\Delta x_{netw}}{\Delta H_{amb}/\Delta x_{amb}} \tau_{netw} \tag{3}$$

where subscripts *netw* and *amb* refer to the values from the block network simulations and those in the regional-scale continuum model, respectively. Since the internodal particle motion involves both section $B$ of the first element and section $A'$ of the second element, the transit time is the sum of the two transit times ${}^{B}\tau$ and ${}^{A'}\tau$ (Figure 2b). The conductivities ($K_{netw}$ and $K_{amb}$) and effective flow porosities ($\phi_{netw}$ and $\phi_{amb}$) are by definition the same. However, block conductivity statistics is determined at four different depth intervals, reflecting the characteristics of the mean of each interval. Therefore the mean conductivity at an

intermediate depth, z, is interpolated by a depth trend, $K(z)$, fitted to the simulated mean values (Figure 3a, in section 3). Furthermore, transit times need to be adjusted by scaling to the depth trend of conductivity with an exponent of 2/3, because in a fractured medium, when subject to a larger stress and decreasing apertures, the flux (and consequently the block conductivity) decreases with a power of 3 (assuming cubic law), whereas the linear flow velocity decreases only with a power of 2, since its effective porosity follows a power of 1. Taking this into account, and setting $\Delta x_{amb} = \Delta x_{netw}$, equation (3) becomes

$$\tau_{amb} = \left( \frac{E[K_j]}{K(z)} \right)^{2/3} \left( \frac{{}^{B}\tau_{netw}}{\Delta\, {}^{B}H_{amb}} + \frac{{}^{A'}\tau_{netw}}{\Delta\, {}^{A'}H_{amb}} \right) \Delta H_{netw}, \tag{4}$$

where $E[K_j]$ is the mean upscaled block conductivity in layer $j$ and $K(z)$ is the interpolated mean conductivity at other depths $z$.

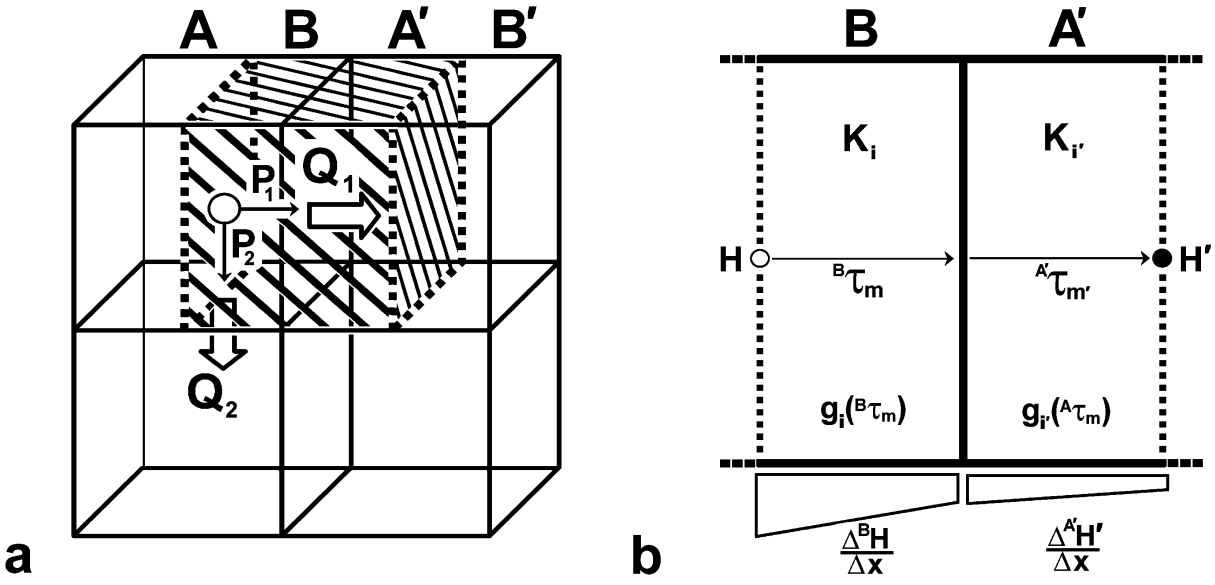


**Figure 2**. (a) Illustration of particle-tracking scheme for an integral finite difference model element with two outward fluxes. (b) A particle movement from a node in an element with conductivity $K_i$ to an adjacent node in an element with conductivity $K_{i'}$ involves sampling distributions linked to realizations $i$ and $i'$.

### 2.3.3 Upstream Conditioning in Transit Time Sampling

As a particle moves from one block element to the next, sampling from transit time distributions for the two neighboring blocks are commonly assumed to be independent random processes. However, one could also expect some correlation between neighboring elements, so that particles traveling along a fast path in one element would travel along a fast path in the next one as well [cf. *Parney and Smith* (1995); *Benke and Painter* (2003)]. In our model, spatial correlation is introduced into the regional stochastic conductivity field, but while this affects the large-scale flow field it does not consider the possibility of channeled transport pathways at the sub-block scale persisting over a distance of several blocks.

To consider such a possibility, the block-scale transit times (i.e., time from the inflow boundary to the outflow boundary) are ranked from the slowest to the fastest, with index $m$ ranging from 1 to 10,000, as described earlier. In transit time sampling, possibilities can then range from autonomous random sampling, where no attention is paid to the previous transit time, to a situation where $m$ is maintained all along a regional particle trajectory. The latter implies that a particle which has followed a fast trajectory in the previous block element continues in a fast trajectory in the next block element as well, and vice-versa. Intermediate alternatives include allowing a small change in the rank, or introducing some type of transport persistence length $d$ where the rank is maintained only for the distance $d$.

To implement this idea in the regional-scale simulations, each particle is assigned an initial rank $m$ at its release, where $m$ is randomly sampled from a uniform distribution and used to identify a transit time in the block-specific distributions. Given the particle rank in an upstream element being $m$, entering the next element the particle is assigned a new rank $m'$; then the alternatives for determining $m'$ are given in Table 1.

**Table 1. Alternatives for sampling particle transit times**

| Alternative | Referred to as | Sampling algorithm |
|---|---|---|
| 1 | Minimum transport channeling | $m$' is autonomous random sampling from uniform distribution [1…10,000], regardless of $m$. |
| 2 | Maximum transport channeling | $m' = m$ for all particle steps |
| 3 | "Dispersion level" specified at element interface | $m' = m + \Delta m$ |
| 4 | Rank maintained for a given "transport persistence length" $d$ | $m' = m$ for a distance $d$ (or $N$ number of elements); then autonomously randomly re-sampled, and returning to $m' = m$ for the next distance $d$. |

The first alternative reflects a minimum level of channeled transport, i.e., only the large-scale channeling arising from the regional correlated conductivity field. This sampling is not linked to previously sampled transit times for the block element; rather, the new rank *m'* is randomly sampled from a uniform distribution.

The second alternative is the other extreme and reflects the maximum level of channeled transport. The sampling rank $m$ randomly assigned to each particle at the onset is kept fixed during the entire particle trajectory and is used for selecting transit times in block-specific distributions of each successive block element. Thus, a particle born into a fast or slow lane is kept on such, even though its velocity may vary along the route.

Neither of the two extremes above seems very realistic, and hence two additional concepts, the alternatives 3 and 4 in Table 1, that allow a transition between the two extremes, are used to examine intermediate levels of transport channeling. These transitional concepts are based on alternative 2, but modified so as to introduce various levels of randomness, in order to regulate the level of transport channeling.

In alternative 3, the sampling rank is increased by $\Delta m$ (which can be positive or negative) each time a particle crosses an element interface. The change $\Delta m$ is determined from a triangular probability distribution, which has an expected value of zero and is bounded by a maximum change, $^{+}/_{-}\ |\Delta m_{max}|$. This maximum change, $|\Delta m_{max}|$, is varied with values 0.01 $M$, 0.1 $M$, 0.25 $M$, 0.5 $M$ and 1.0 $M$, where $M$ is the maximum rank, and thus represents high-to-low levels of channelized transport.

Alternative 4 in Table 1, is the case for "tracer-transport persistence length," $d$, which is longer than the block scale, $\Delta x$, so that $d = N \times \Delta x$, where we define $N$ as "tracer-transport persistence". In this alternative, the sampling rank $m$ is kept fixed over a distance of $N$ successive elements. After $N$ elements have been traversed, a new rank $m'$ is sampled independently, as in alternative 1. Then the particle moves along the next set of $N$ successive block elements with a fixed $m$ value. For a given simulation of regional tracer transport ($10^6$ particles), $N$, is treated as a random variable sampled from a uniform distribution, ranging from 1 to $2N$-1. However, to avoid cases where a choice of $N$ steps would lead the particle to go beyond the exit boundary, $N$ is cut back so that it always ends at the boundary. Thus the mean of the random $N$ values, $N_A$, is always less than $N$ for large cases of $N$. Channelized transport is examined for various average "transport persistence," $N_A$, ranging from 390.4 to 1.0, which represent maximum to minimum channeling levels.

## 3. Example Application to Field Data

The use of the model developed is demonstrated as part of a model cross-comparison study within the international DECOVALEX project (*Tsang et al.*, 2003). The database used for this comes from the Sellafield site in England, as summarized by *Andersson and Knight* (2000). Particle transport from a potential deep nuclear waste repository is simulated in a vertical cross section, as shown in Figure 3a. The range of particle transit times from the underground repository to the sea is to be simulated. No-flow boundaries are assigned for boundaries at $x$ = 5000 m, $x$ = 0 m, based on symmetry considerations at water divide, and at $z$ = 1000 m, based on the very low conductivity at this depth, as often can be assumed in fractured media. Constant-head boundary conditions are assigned at the top of the model, corresponding to the mean levels of the groundwater table and the sea. There is a vertical fault in the middle of the domain, while the remaining part of the medium is "average" fractured rock. This rock also has a depth trend in conductivity caused by fracture closure with increasing stress at greater depths. It is the "average" fractured rock that needs upscaling for the regional-scale transport model, regarding both its hydraulic and transport properties. Due to the domain geometry, these properties are characterized (see Figure 3a) at different depth levels (e.g., $g(K_j)$ where $j$ refers to the depth level), and at a larger support scale in a region having less influence on transport (e.g., $g_{45\,m}(K)$), which will be explained in the following sections.

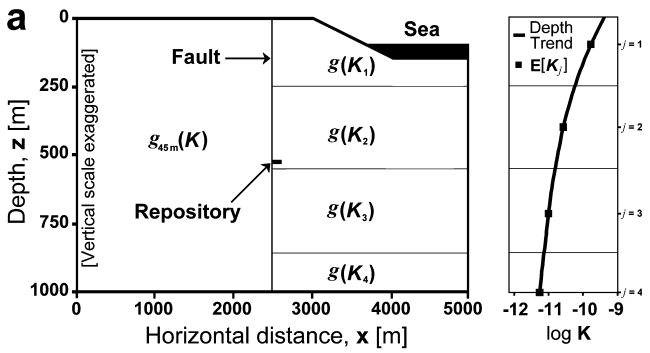


**Figure 3a.** Regional-scale hydraulic flow modeling and particle-tracking domain: conceptual model with input conductivity distributions, $g(K_j)$ and $g_{45\,m}(K)$, and the interpolated depth trend $K(z)$.

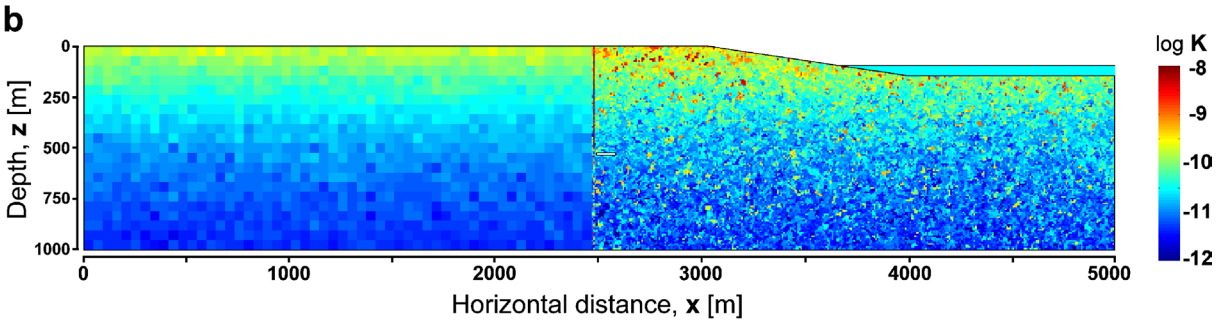


**Figure 3b.** One stochastic realization of the regional-scale conductivity field.

### 3.1 Upscaling of Fracture Networks

#### 3.1.1 Data

Our approach is based on fracture network modeling at the block scale. Multiple three-dimensional fracture network realizations are generated, and input data for these network realizations are statistical distributions of geologically observed fracture orientations, lengths, density, and intersection termination percentage, taken from the Nirex databases as summarized in *Andersson and Knight* (2000). Statistical fracture transmissivity distributions are estimated using a probabilistic analysis of hydraulic well test data, according to the method introduced by *Osnes et al.* (1988). Details of these fracture and hydraulic conductivity

data and their analysis for hydraulic fracture network modeling are given in *Öhman and Niemi* (2003) and will not be repeated here.

To account for decreasing conductivity with depth, principal stresses, as reported by *Nirex* (1997d), are used to calculate the stress regimes at various depths. These in turn are used to correct the fracture transmissivities at these depths, as hydraulic data are only available at a limited depth interval (from 635 to 790 m). In doing so, fracture transmissivities are adjusted, such that the relation between the geometric mean transmissivity and an anisotropic stress-field satisfy an empirical fracture-closure relationship based on an analysis of core loading-unloading data. This latter data comes from *NGI* (1993). The step of adjusting fracture transmissivity depending on its orientation in the ambient stress-field is further explained in *Öhman et al.* (2004).

### 3.1.2 Hydraulic Upscaling at Block Scale

Block-scale flow modeling was conducted for 4 × 100 ($j \times i$) fracture network realizations to generate hydraulic conductivity distributions as input to the regional-scale flow calculations. For this purpose, the computer codes FracMan (*Dershowitz et al.,* 1998) and MAFIC (*Miller et al.,* 1999) were used, which allow modeling flow and particle transport in complex three-dimensional fracture geometries. The simulations were carried out as discussed in section 2.3.1, and are further described in *Öhman and Niemi* (2003). The horizontal and vertical components of equivalent conductivity were extracted from each simulated conductivity tensor to form input conductivity distributions for generating the regional-scale stochastic continuum flow model. Four different block scale conductivity distributions were determined, $g(K_j)$, which correspond to the four different depth levels $j$ = 100 m, 400 m, 713 m, and 1000 m.

For computational reasons, a statistical conductivity distribution was also determined at 45 m block scale, $g_{45\,m}(K)$. This distribution is intended for regions where the heterogeneity effects are of less importance (Figure 3) because particles are not expected to pass through them. For this reason, an additional upscaling was carried out to further upscale the 7.5-m scale conductivities to effective conductivities at 45-m scale. This upscaling was done based on stochastic continuum modeling and is presented in detail in *Öhman et al.* (2003).

### 3.1.3 Upscaling Particle Transport at Block Scale

The first attempt to upscale transport properties was made to see whether a continuum-type dispersion tensors could be determined at the same block-scale as for continuum representation of hydraulic conductivity. Particle tracking was initially performed through 30 of the 100 fracture networks at the block scale. It was done in a similar way as for upscaling the hydraulic conductivity (*Öhman and Niemi*, 2003). For each realization, the flow field was first solved for a $15 \times 7.5 \times 7.5$ m$^3$ region in various directions, $\theta$, by gradually rotating a hydraulic gradient in a vertical cross section (Figure 4). The gradient was given a magnitude of 0.05, which corresponds to the average regional gradient in the regional-scale model. No-flow conditions were applied to the boundaries parallel to the regional-scale modeling plane.

The block region (side-length 7.5 m) being studied is embedded in a somewhat larger flow field (Figure 4). This is to provide "guard zones" (*Jackson et al.*, 2000) that reduce the risk of shortcuts to adjacent boundaries. Ten thousand particles were released from a $2 \times 2$ m$^2$ surface at the center of the inflow boundary and collected at outflow boundaries. Particle transit time statistics were sampled at various longitudinal distances, $L$, and at various times, $t$. As an example, Figure 4 also shows a set of calculated particles trajectories. Note that most particles are channeled along a high-velocity path and generate transit times around 30 years, whereas for others it can exceed 80 years.

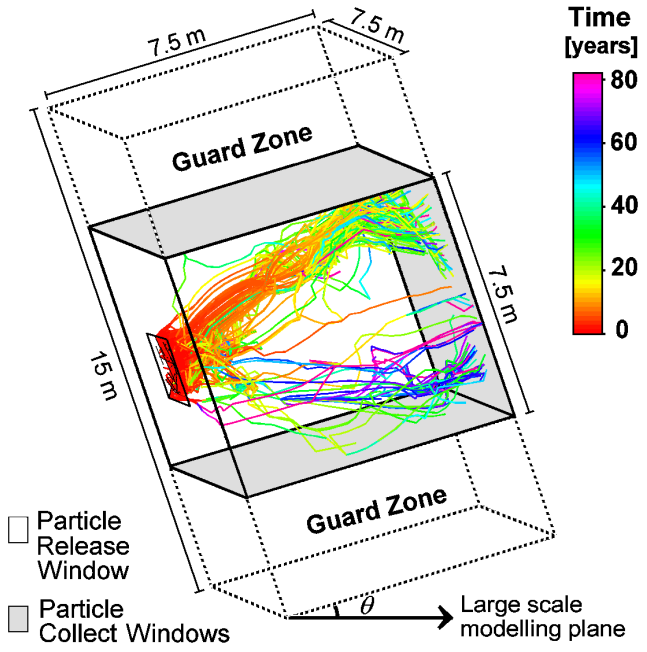


**Figure 4.** Flow and transport regions vertically rotated by an angle $\theta$ to obtain particle dispersion characteristics and a sample of achieved particle trajectories.

As will be discussed in the "Results" section (section 4) the results of the above analysis shows that particle dispersion is considerably more heterogeneous than hydraulic conductivity at the same scale. Therefore a continuum dispersion tensor representation could not be found, and hence, our approach, as described in section 2.2.2, was used. The discrete particle travel statistics are transferred directly to the regional-scale model.

Particle tracking was conducted in vertical and horizontal directions only, in accordance to the structure of the regional-scale finite difference model into which the information was to be transferred. The same 4 × 100 fracture network realizations that were used for flow simulations described in section 3.1.2, were used here. Again, 10,000 particles were released to estimate distributions of transit time $\tau$. Or more precisely, the transit time distributions were determined separately for the upstream and downstream sections of the network blocks $g({}^{A}\tau)$ and $g({}^{B}\tau)$, such that ${}^{A}\tau_m + {}^{B}\tau_m = \tau_m$.

### 3.2 Regional-Scale Simulations

#### 3.2.1 Flow Simulations

Based on the upscaled data, regional-scale stochastic continuum simulations were carried out. A sample conductivity realization is shown in Figure 3b. The region to the right of the fault zone was discretized into cubic elements identical to our block scale (side length of 7.5 m), to provide a consistent transfer of the heterogeneity characteristics. For the region to the left of the fault zone, coarser elements of dimensions $45 \times 45 \times 7.5$ m$^3$ were used and assigned the separate conductivity distribution $g_{45\,m}(K)$ (Figure 3; section 3.1). Since no particle tracking will take place within this region, the particle transport characteristics were not upscaled to this support scale.

First, four correlated stochastic conductivity fields for the region were generated with the GSLIB algorithm for the four different depth intervals (0 to 250 m, 250 m to 550 m, 550 to 856 m, and 856 to 1000 m), using the upscaled conductivity statistics $g(K_j)$ and an exponential variogram with a correlation length of 18 m, based on a separate variogram upscaling study presented in *Öhman et al.* (2003). Then, the mean conductivity of the fields was adjusted to the interpolated depth trend, $K(z)$ in Figure 3a, to obtain smoothly varying mean conductivity at all intermediate depths, $z$. Finally, each generated conductivity value was indexed to its actual network realization of origin, in order to link each element to its corresponding particle transit time distribution. The procedure described was repeated, and 30 regional-scale realizations were generated. Then the steady state flow field was solved for each.

#### 3.2.2 Regional-Scale Particle Tracking

Regional-scale particle tracking was then carried out for steady state flow-fields for the 30 realizations at the regional scale. For each realization, $10^6$ particles were released at the repository (Figure 3a), and their breakthrough at the sea was observed and analyzed. The impact of different levels of superimposed channelized transport, represented by the four alternatives in the sampling algorithms (Table 1, section 2.3.3) was then explored.

## 4. Results

### 4.1 Upscaling Network Characteristics

#### 4.1.1 Applicability of Dispersion Coefficient at Block Scale

The results of upscaling the flow in the block-scale fracture networks are discussed in detail in *Öhman and Niemi* (2003) and will not be repeated here. Those results showed that most block conductivities could be reasonably well represented by means of a continuum conductivity tensor at the 7.5 m block scale. The criterion for this was that the directional conductivity as a function of orientation could be described by an ellipse when plotted as $\sqrt{1/K}$ versus orientation angle $\theta$ plot, or smoothly fit to a tensor description when expressed as a $K$ versus $\theta$ plot (*Harrison and Hudson*, 2000).

As expected, the particle breakthrough results appear much more heterogeneous than the corresponding flow simulations, which is similar to the findings of e.g., *Endo et al.* (1984). Figure 5b shows transit time at 16, 50 and 84 percentiles, $\tau_{16}$, $\tau_{50}$ and $\tau_{84}$, for various orientations, $\theta$, for a typical fracture network realization, based on 10,000 particles released. For comparison, the corresponding hydraulic conductivity versus rotational angle plots for the same network is shown in Figure 5a. It can be seen that while the conductivity shows a definite homogeneous behavior, the transport behavior is highly heterogeneous with orientation and cannot be represented by a dispersion tensor.

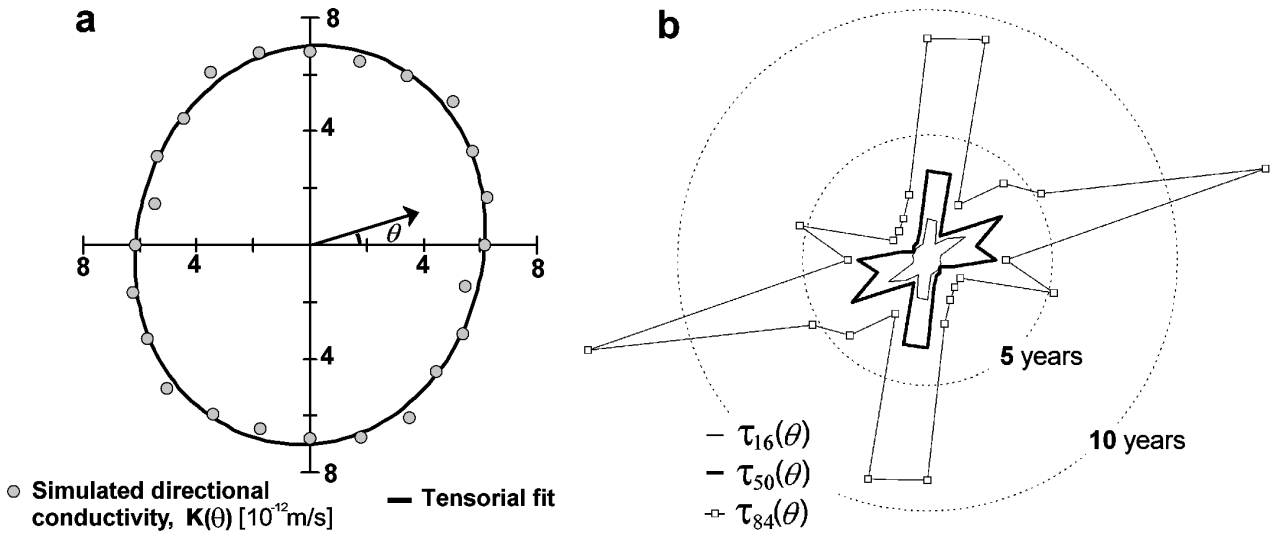


**Figure 5.** (a) Typical directional hydraulic conductivity as a function of rotation angle $\theta$ for a realization and (b) its corresponding transit time percentiles $\tau_{16}$, $\tau_{50}$, and $\tau_{84}$ as a function of $\theta$.

Two examples of particle breakthrough curves, along with fitted analytical solutions of the one-dimensional ADE, are shown in Figure 6. Approximately 94% of the breakthrough curves for investigated realizations could be fairly well fitted with the one-dimensional ADE, as the example shown in Figures 6a and b for a particular realization, while the remaining could not (e.g., Figures 6c and d). The procedure for determining dispersion coefficients is based on equations (5) and (6), and described in section 4.3 below.

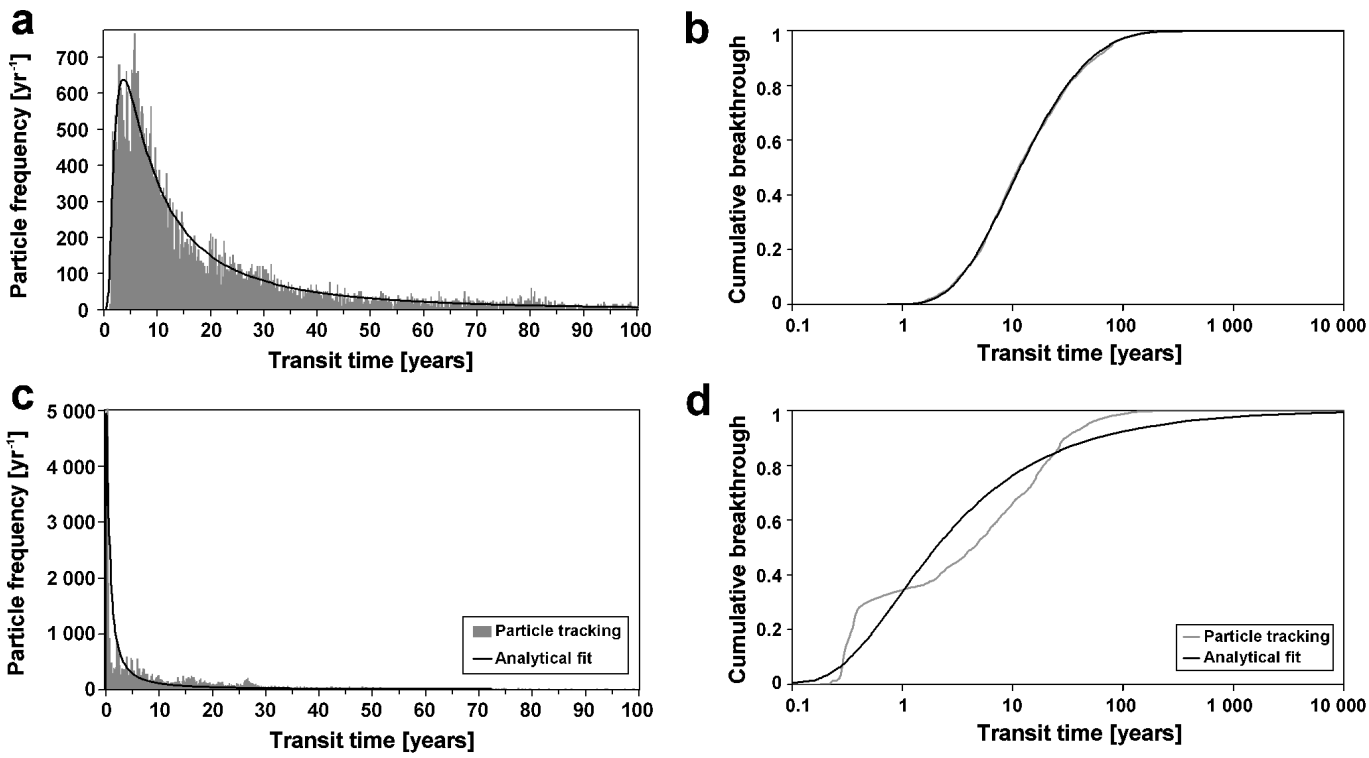


**Figure 6.** Breakthrough curves and analytical fits for two sample fracture network realizations; one is well-fitted, (a) and (b), and the other poorly fitted, (c) and (d).

A histogram of obtained block-scale dispersivities $\alpha = L/Pe$ from a fit with 1-D ADE is shown in Figure 7. It reveals a lognormal distribution. Note that dispersivity values > 100 correspond to realizations where the agreement between breakthrough data and the ADE model was poor, as determined by means of a Kolmogorov-Smirnov test (e.g., Figures 6c and d). This indicates that realizations with the largest heterogeneity (large $\alpha$), are also the least "smooth" and are hardly described adequately by means of a continuum dispersivity.

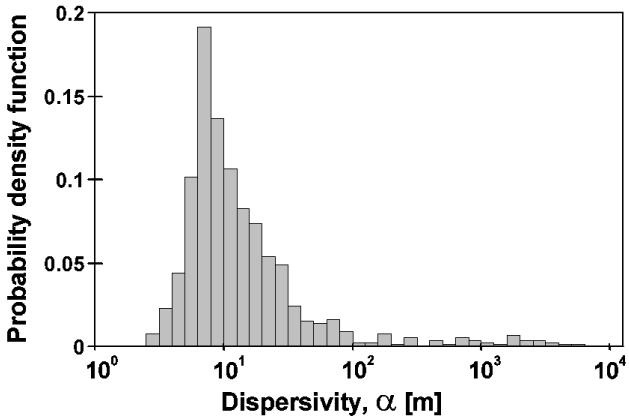


**Figure 7.** Histogram of block-scale dispersivities (please note: values with $\alpha > 100$ correspond to cases of bad agreement between the analytical ADE and the simulated fracture network results, as shown in Figures 6c and d).

### 4.1.2 Particle Transit Time Distributions

One conclusion drawn in the previous section was that solute transport cannot be represented by means of dispersion tensors at the 7.5 m block scale. Thus, we apply our model by taking the distributions of particle transit times themselves and transfer them to the regional-scale model. These transit time distributions have a wide spread. Figure 8 shows the 84$^{th}$, 50$^{th}$ and 16$^{th}$ percentiles of the simulated particle transit times as a function of simulated block conductivity. Inspection of the results shows that, while there is a clear correlation between conductivity and transit time (with low conductivity corresponding to long transit times), there is also a wide spread in transit time values for a given conductivity.

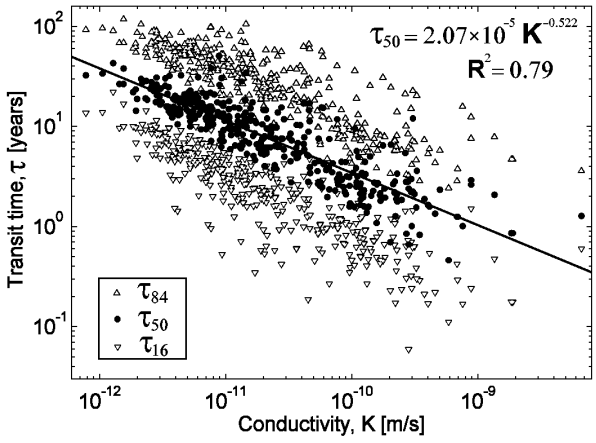


**Figure 8.** Simulated particle transit times (84$^{th}$, 50$^{th}$, and 16$^{th}$ percentiles) as a function of block-scale conductivity (upscaled values for 7.5 m network blocks).

### 4.2 Results from Regional-Scale Particle Tracking

The impact of the superimposed transport channeling (Table 1) is demonstrated in Figure 9, for 100 out of $10^6$ particles released onto the flow field of one sample regional stochastic realization. The minimum level of transport channeling, alternative 1 in Table 1, is shown in Figure 9a and compared to maximum transport channeling, alternative 2, shown in Figure 9b. The colors indicate the elapsed time since particle release. As can be seen, alternative 1 causes very little longitudinal spreading compared to the extraordinary longitudinal spreading obtained by alternative 2. As discussed in section 2.3.3, alternative 1 is the case of random sampling at every step, whereas alternative 2 maintains long-range persistent particle pathways that can be associated to occurrence of large scale transport channeling, such as in the case of presence of fracture zones, i.e., features that can be expected to produce very large longitudinal dispersion, with both very fast and very slow transit times.

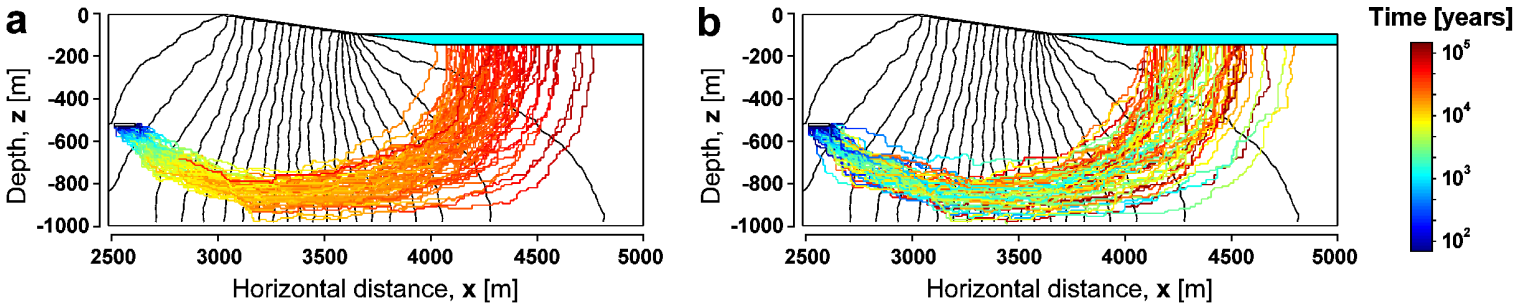


**Figure 9.** Simulated particle transit times for 100 pathways along with corresponding head fields for one stochastic realization: (a) for alternative 1, and (b) for alternative 2.

Breakthrough curves obtained from regional-scale particle tracking, for the intermediate alternatives 3 and 4 in Table 1, are shown in Figures 10a and b, respectively. Figure 10a shows results for different $|\Delta m_{max}|$-values, i.e., variable "dispersion levels" that modify the sampling rank at element interfaces, and Figure 10b shows results for different values for $N_A$, which are conceived as the average "transport persistence." Inspection of the results in Figures 10a and b shows that the completely random alternative, without additional transport channeling ($|\Delta m_{max}| = 1.0$ or $N_A = 1$), has the narrowest breakthrough with a late first arrival, while the maximum channeling ($|\Delta m_{max}| = 0.0\ M$ or $N_A$ = infinite) has an early first

arrival and a long tail. Intermediate values for $|\Delta m_{max}|$ and $N_A$ successfully represent transitions between these two limits.

Of the two cases, we can argue that the case with a specified transport "persistence length" (Figure 10b) is more reasonable, as it is more physically based. The other alternative is somewhat artificial since the deviations in path rank are only allowed at element interfaces, which in turn are artificial boundaries, while the "transport persistence length," or "correlation distance," is a physical entity that in principle could be measured or estimated from field data. We therefore use the results in Figure 10b for further analyses.

Figure 10c shows the results from Figure 10b fitted to the one-dimensional ADE equation. The solution for one-dimensional breakthrough after an instantaneous pulse injection (e.g., *Käss*, 1998) can be expressed for $n_p$ released particles as

$$n(L,t) = \frac{n_p}{t_0\sqrt{\frac{4\pi}{Pe}\left(\frac{t}{t_0}\right)^3}} \exp\left[\frac{\left(1-\frac{t}{t_0}\right)^2}{\left(\frac{4}{Pe}\frac{t}{t_0}\right)}\right], \tag{5}$$

where $n(L,t)$ is the number of particles at distance $L$ and at time $t$, $n_p$ is the total number of particles released at the source, $t_0$ is the mean transit time, and $Pe$ is the Peclet number, defined by

$$Pe = \frac{v\,L}{D_L} \tag{6}$$

where $D_L$ is the longitudinal dispersion coefficient, $v$ is the mean flow velocity, and $L$ is the distance between injection and observation. The results in Figure 10b were fitted to equation (5) by fitting the two free parameters of mean transit time, $t_0$ and Peclet number, $Pe$. The best fits were found by minimizing the root-mean-square error between the simulated breakthrough curves and the analytical model.

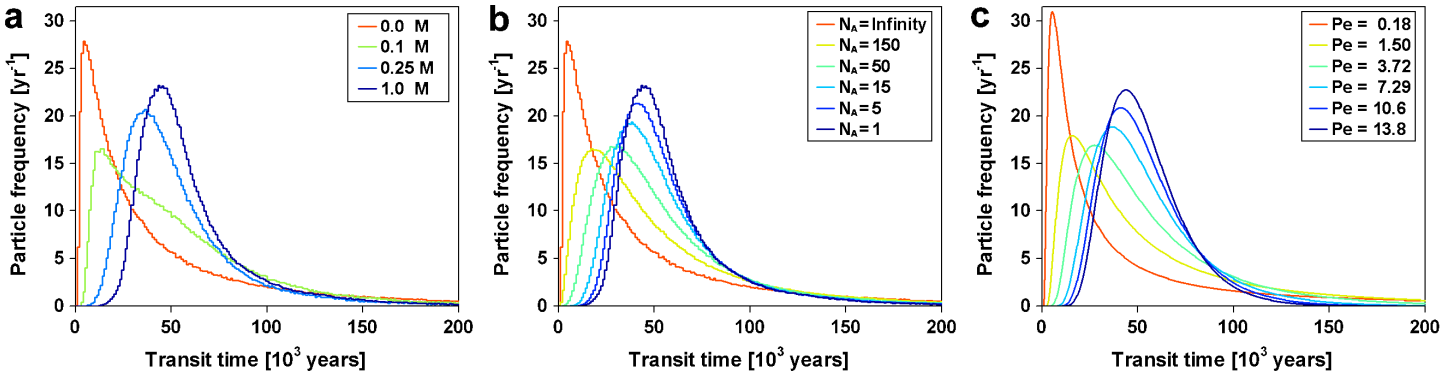


**Figure 10.** Simulated particle breakthroughs: (a) for various "dispersion levels," $|\Delta m_{max}|$, alternative 3 in Table 1, (b) for various ranges of "transport persistence," $N_A$, alternative 4 in Table 1, and (c) the one-dimensional ADE fitted to simulated results in (b).

To see how well the simulated results can be fitted the analytical ADE model, six cases are shown in Figure 11. Visual inspection of the results indicates that the fit is best for the intermediate range of $N_A$-values and *Pe*-numbers, while for very low *N,* the ADE model produces too much spreading and at high $N_A$ (extreme channeling), the ADE model produces a more extreme peak than the simulation results. A quantitative evaluation of the fitting error showed that the best fits were obtained for $N_A$-values ranging from 30 to 100, which correspond to "transport persistence lengths," *d*, of 225 to 750 m. It can, however, be concluded that throughout the range of $N_A$ values, the fits are relatively good when judged by visual inspection.

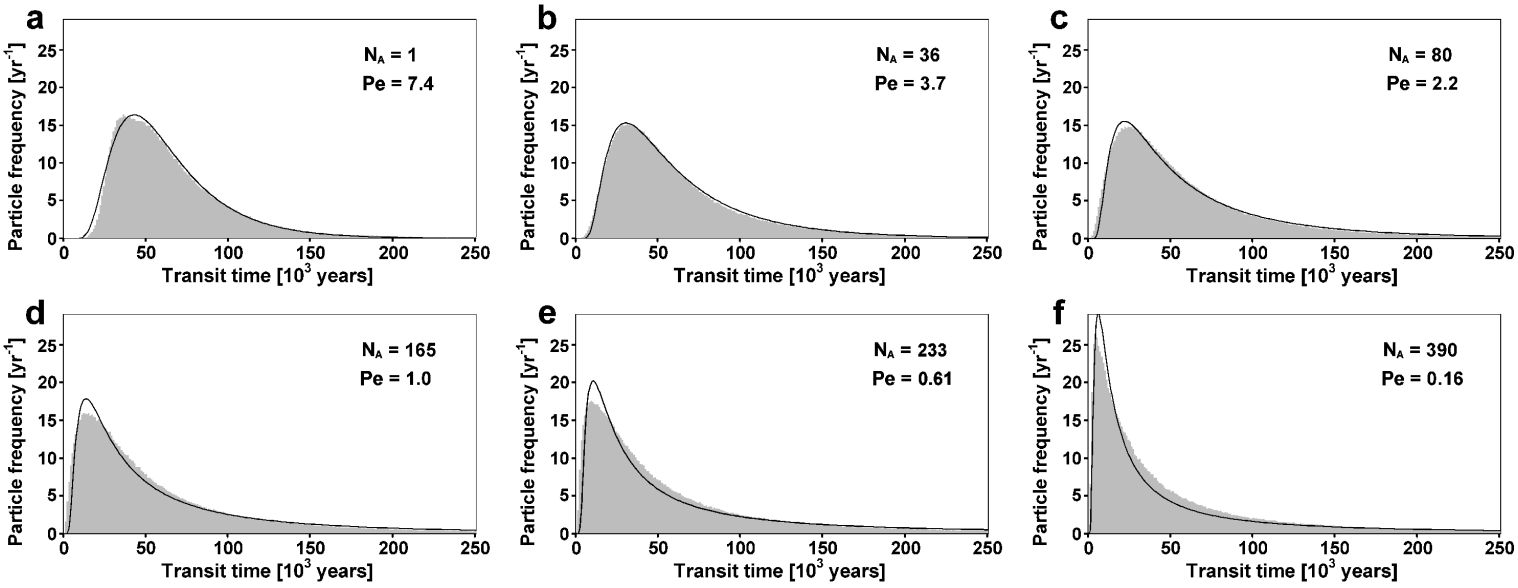


**Figure 11.** Histograms of simulated particle breakthrough and their corresponding analytical fits for a range of average "transport persistence," $N_A$.

The fitted Peclet number is given as a function of the connected path length, $N_A$, in Figure 12a. Inspection of the results shows that high $N_A$ values (i.e., long connected path lengths) correspond to low Peclet numbers and therefore (as all other terms in equation (5) are constant) to high dispersion coefficients. Conversely, short connected path ranks correspond to low dispersion. This is a natural result, because long persistence lengths can be seen as effect of strong and spatially correlated heterogeneities, which are expected to increase dispersion. It is of interest to note that $N_A$ values larger than 165 yield "unphysical" Peclet numbers of less than one, which nevertheless fit the computed tracer breakthrough curve quite well (see Figures 11e and 11f).

The other fitting parameter, mean transit time, $t_0$, is relatively constant for a large range of connected path lengths. However, it is not a very useful or readily measurable parameter, and therefore of lesser practical interest than the dominant peak-arrival time. The dominant peak-arrival times are plotted as a function of the "transport persistence" in Figure 12b. The result shows that the longer the connected path length, the faster the peak arrival.

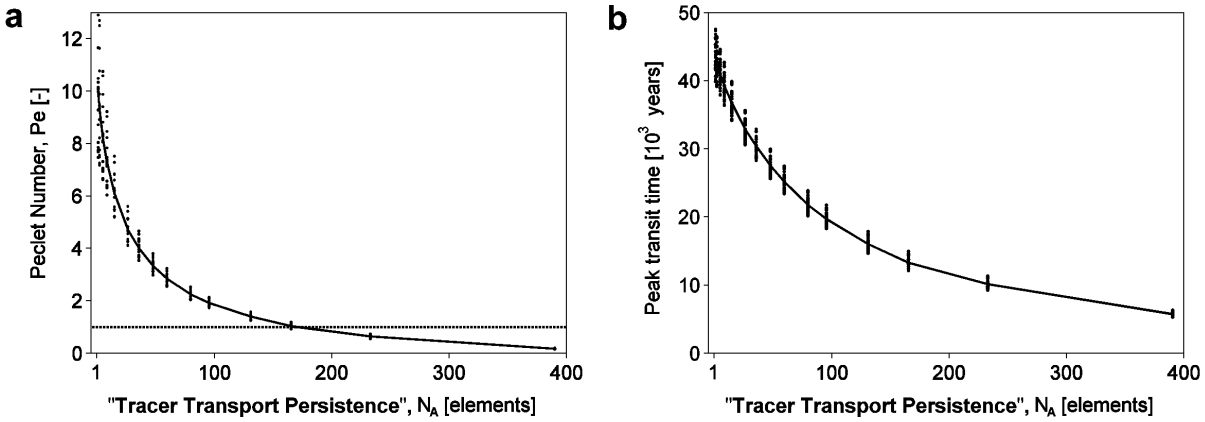


**Figure 12**. (a) Peclet number and (b) dominant peak-arrival time as a function of average "tracer transport persistence," $N_A$, determined from 30 regional-scale simulations.

### 4.3 Regional-Scale Dispersion Coefficient

Figure 13 shows the relationship between macroscale longitudinal dispersion coefficient and $N_A$. Inspection of the results shows a very strong linear correlation between the two parameters. It has been shown earlier by *Gelhar and Axness* (1983) that a direct relation exists between correlation length of the log conductivity field and macroscale dispersion coefficient $A_L$ (see, e.g., *Domenico and Schwarz*, 1998)

$$A_L = \frac{\sigma^2{}_Y \lambda}{\gamma^2} \tag{7}$$

where $Y$ is the log-transformed hydraulic conductivity ($Y = \ln K$), $\sigma^2{}_Y$ and $\lambda$ are the variance and correlation length of $Y$, and $\gamma$ is a flow factor that, according to *Dagan* (1982) (see *Domenico and Schwarz*, 1998), can be approximated by one.

In the present study, the correlation of conductivity is kept constant, and thus the increase in dispersion coefficient in Figure 13 arises from the "persistence" in transport pathways, which are superimposed on the correlated conductivity field.

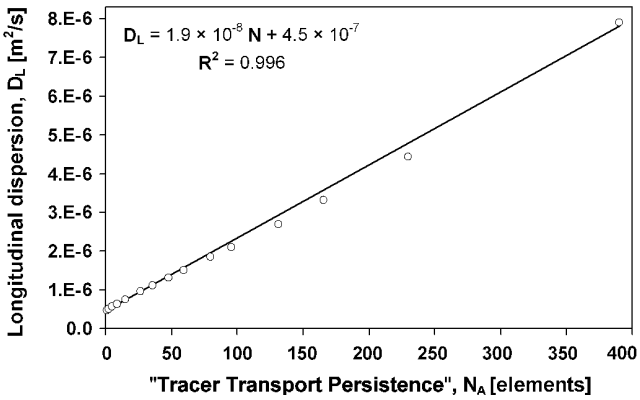


**Figure 13.** Mean longitudinal macroscale dispersion coefficients as a function of average "tracer transport persistence," $N_A$.

While the present data with its depth trend is too non-ideal to draw any general conclusions about the form of the relationship in Figure 13, it is still of interest to analyze, in a preliminary sense, both the slope $k$ and the minimum value $D_0$ (i.e., the intercept with the ordinate axis of the fit). We found that $k = 1.9 \times 10^{-8}$ m$^2$ s$^{-1}$ element$^{-1}$ and $D_0 = 4.5 \times 10^{-7}$ m$^2$/s.

### 4.3.1 Background Dispersion due to Heterogeneous Conductivity Field

The minimum value of the dispersion coefficient at the lower limit of $N_A = 1$ can be considered to represent some kind of background dispersivity on the regional scale. To confirm this background dispersion, we simulated the regional particle tracking once more by replacing the block-scale transit time distributions by their individual block-scale mean values. In this way, all "internal" block-scale variability was eliminated and the regional particle breakthrough then only reflects dispersion, arising from the heterogeneity in the regional-scale flow field (due to the correlated conductivity field and its depth-trend). The results from 30 realizations were again fitted to the analytical ADE. The resulting dispersion coefficient statistics had a mean of $3.9 \times 10^{-7}$ m$^2$/s and a standard deviation of $8.5 \times 10^{-8}$ m$^2$/s, which is in good agreement with the background value in Figure 13. A simple substitution of the data values into equation (7) gives a value $6.4 \times 10^{-8}$ m$^2$/s, which is smaller than the background dispersion coefficient in Figure 13 but is reasonable, as the nonstationarity with depth can be expected to increase dispersion.

### 4.3.2 Dependency of Dispersion Coefficient on Transport "Persistence Length"

To further analyze the characteristics of the linear relationship in Figure 13, we show here that for a one-dimensional domain, its macroscale dispersion coefficient can be presented as a linear function of the block-scale dispersion coefficients.

Assume that there exists an effective dispersion coefficient at the defined block-scale (in our case, 7.5 m), where the dispersion coefficient $D_{LB}$ can be defined as (see, *Domenico and Schwartz*, 1998)

$$D_{LB} = \sigma_{tB}^2 \frac{v_B^2}{2t_B}, \tag{8}$$

where $\sigma_{tB}^2$ is the variance of particle breakthrough (variance in particle transit time through the block), $v_B$ is the average linear groundwater flow velocity, and $t_B$ is the mean transit time through the block. Then, based on general rules concerning the variance for a sum of random variables with known variances, the variance in transit times through the entire one-dimensional domain of $N_0$ connected blocks can be calculated based on the block-scale variance, $\sigma_{tB}^2$.

The variance in transit time for "persistent passage" through a series of $N$ connected blocks (i.e., thus fully correlated transit times, such that all covariance terms are equal to the variance) is determined by the variances for the $N$ dependent populations:

$$\sigma_{tN}^2 = \left( \sum_1^N \sigma_{tB} \right)^2 = N^2 \, \sigma_{tB}^2 . \tag{9}$$

Second, the total variance in transit time through $N'$ independent such segments, at a scale beyond the "persistence length", is determined by summing the variances of $N'$ independent distributions, i.e., all covariance terms are here equal to zero,

$$\sigma_{tN'}^2 = \sum_1^{N'} \sigma_{tN}^2 = N' \, \sigma_{tN}^2 , \tag{10}$$

Combining these two, the total variance $\sigma_t^2{}_{N0}$ of a sequence of $N_0$ distributions (in our case block transit times), containing correlated subgroups (with $N$ inter-correlated distributions each) yields

$$\sigma_{t\,N0}^2(N) = \sum_{1}^{N_0/N} \left( \sum_{1}^{N} \sigma_{t\,B} \right)^2 = N\ N_0\ D_{LB} \frac{2t_B}{v_B^2}. \tag{11}$$

For $N = 1$ (nonpersistence) $\sigma_t{}^2{}_{N0}\,(1) = N_0\ \sigma^2{}_{tB}$, while for $N = N_0$ (persistence covers the entire domain) $\sigma_t{}^2{}_{N0}\,(N_0) = N_0^2\ \sigma^2{}_{tB}$. Then, in analogy with equation (8), the dispersion coefficient for the regional-scale domain with $N_0$ blocks becomes

$$D_{L0}(N) = \frac{v_0}{2t_0} \sigma_{t\,N0}^2(N) = N \frac{v_0^2}{v_B^2} \frac{2t_B}{2t_0} N_0\ D_{LB}, \tag{12}$$

where $t_0$ is mean transit time through the regional-scale flow domain and $v_0$ is velocity through this domain. Note that, for a one-dimensional stream tube, average velocity and block velocity must be equal, $v_0 = v_B = L_0/t_0$ and $t_0 = N_0 \times t_B$, where $L_0$ is mean trajectory length through the entire region (in our case $L_0 = N_0 \times 7.5$ m), which reduces equation (12) to

$$D_{L0}(N) = N\ D_{LB}. \tag{13}$$

In other words, equation (13) states that for a one-dimensional transport path, the total longitudinal dispersion coefficient is a linear product of the number of intercorrelated blocks and the block-scale dispersion coefficient. Then, for the data in Figure 13, this would mean that the proportionality coefficient $k = 1.9 \times 10^{-8}$ m$^2$ s$^{-1}$ element$^{-1}$ is equated with some type of representative block-scale dispersion coefficient.

To test whether this is the case, we use the geometric mean of all block-scale dispersivities $\alpha_B$, determined by fitting block-scale particle-tracking results to the one-dimensional ADE (section 4.1.1), as the representative block dispersivity. This is justified because the histogram in Figure 7 is relatively log-normal in appearance, in spite of the "tail"

at high dispersivity, where the agreement with the ADE model also was its worst. Using this geometric mean dispersivity, $\alpha_g$ (= 12.6), as the basis for the representative block-scale dispersion coefficient, we get for $D_{LB} = \alpha_g v_0 = \alpha_g L_0/t_0 = 1.89 \times 10^{-8}$ m$^2$/s. This is in excellent agreement with the result in Figure 13, indicating that the relationship in equation (13) is indeed a promising model for transport-related scaling effect in regional-scale transport.

## 5. Summary and Conclusions

A regional-scale transport model is proposed that is applicable to nonstationary and statistically inhomogeneous fractured media: provided that hydraulic flow, but not necessarily solute transport, can be approximated by equivalent continuum properties at some block scale. Based on the available hydraulic and fracture geological data, block-scale fracture network realizations are generated at a scale defined by a valid tensorial continuum representation for conductivity. Block conductivity values and corresponding particle transit time distributions are then determined for each of the network realizations at this block scale. These are in turn used as input for a regional-scale model. In the regional-scale model, flow is solved in a stochastic continuum framework, while transport is solved by means of a random-walk procedure. In random walk, the time taken for a particle to traverse an element is sampled from a transit time distribution linked to that particular block element.

For each network realization *i*, an effective conductivity tensor is determined at the block scale. For the same realization, we also obtain a corresponding distribution of transit times. Results of multiple realizations then provide input to tracer transport calculation at the regional scale with many block elements. Now, to what extent the sampling of transit time distributions for each block element in the regional-scale model should be linked to an upstream element is not obvious. Possible alternatives for sampling the transit time distributions range from a completely random sampling (where no attention is paid to the previous history), to a situation where a path rank *m* is strictly maintained and transport paths are correlated throughout the model domain. In the latter scenario, a particle that for example has followed a fast pathway in the previous numerical element is assigned a fast pathway in the next element as well. Applying this method to a realistic sample data set, our simulations demonstrate that the choice of connectivity structure is important for regional-scale model predictions. The peak arrival time can vary by almost an order of magnitude between the most

extreme scenarios. Intermediate levels of channeled transport is modeled by (alternative 3) allowing a small change in the path rank at the element interfaces and (alternative 4) introducing a transport "persistence length," where the path rank is maintained for a certain distance.

While both alternatives were tested on the field data set and showed a meaningful transitional behavior between the two extreme scenarios, alternative 4 was chosen to be analyzed further. The regional-scale breakthrough curves from this approach were then fitted to the one-dimensional ADE, in order to determine regional-scale dispersion coefficients, or alternatively, Peclet numbers. The data agreement with the analytical ADE-model was satisfactory throughout the range of examined "transport persistence distances" and was best for intermediate ranges. For very low $N$ values, the ADE model produces too much spreading, whereas very high $N$ values (extreme channeling) produce a more extreme peak than the simulated breakthrough curve.

Further analysis of the results shows that there is a clear linear correlation between the regional-scale dispersion coefficient and the "transport persistence distance." This is because large persistence distances cause larger spread of fast and slow particles, which in turn increase the dispersion coefficient. The macroscale dispersion coefficient $D_L$ could be linked to the connective path length or average "transport persistence distance," quantified by a number of elements, $N_A$, through

$$D_L = D_0 + N_A \, D_{LB} \, . \tag{14}$$

where $D_0$ is a background dispersion, caused by the underlying regional correlated conductivity field and the depth trend in conductivity, and $D_{LB}$ is an effective block-scale dispersion coefficient. This is found to be equal to the product of the geometric mean of block-scale dispersivities and the mean velocity from the source to the observation point ($\alpha_g \, v$). This is an interesting finding, providing potentially a promising tool for making estimates concerning regional scale transport based on detailed scale data, even without simulations. This deserves further investigation including field studies to confirm its validity.

**Acknowledgments.** This work has been carried out as part of an international collaboration project DECOVALEX and has been supported by the Finnish Radiation and Nuclear Safety Authority (STUK). We wish to thank STUK and especially Dr. Esko Eloranta for financial support and interest in this work. Further thanks go to many of the collaborators within the DECOVALEX group and coworkers at the Department of Earth Sciences at Uppsala University, especially Mr. Niclas Bockgård, for their valuable comments during the course of this work. The third author would like to acknowledge the support of the Director, Office of Science, Office of Basic Energy Sciences, Geoscience Program of the U.S. Department of Energy, and the Japan Nuclear Development Cycle Institute (JNC), under the Binational Research Cooperative Program between JNC and U.S. Department of Energy, Office of Environmental Management, Office of Science and Technology (EM-50), under Contract No. DE-AC03-76SF00098 with Ernest Orlando Lawrence Berkeley National Laboratory. Finally, we wish to thank Golder Associates for access to the FracMan and MAFIC software packages.

## References

Abbo, H., U. Shavit, D. Markel, and A. Rimmer (2003), A numerical study on the influence of fractured regions on lake/groundwater interaction; the Lake Kinneret (Sea of Galilee) case, *J. Hydrol.*, *283*, pp. 225-243.

Andersson, J. and J. L. Knight (2000), The THM Upscaling Bench Mark Test 2 - Test Case Description, edited by J. L. Knight, United Kingdom Nirex Limited, Harwell (www.decovalex.com).

Andersson, P., J. Byegård, E.-L. Tullborg, T. Doe, J. Hermanson and A. Winberg (2004), In situ tracer tests to determine retention properties of a block-scale fracture network in granitic rock at the Äspö Hard Rock Laboratory, Sweden, *J. Contam., Hydrol.*, *70*, pp. 271-297.

Becker, M. W. and A. M. Shapiro (2000), Tracer transport in fractured crystalline rock: Evidence of nondiffusive breakthrough tailing, *Water Resour. Res.*, *36*(7), pp. 1677-1686.

Berkowitz, B. (2002), Characterizing flow and transport in fractured geological media: A review, *Adv. Water Resour.*, *25*, pp. 861-884.

Bruderer, C. and Y. Bernabe (2001), Network modeling of dispersion: Transition from Taylor dispersion in homogeneous networks to mechanical dispersion in very heterogeneous ones, *Water Resour. Res.*, *37*(4), pp. 897-908.

Benke, R. and S. Painter (2003), Modeling conservative tracer transport in fracture networks with a hybrid approach based on the Boltzmann transport equation, *Water Resour. Res*., 1324, doi:10.1029/2003WR001966.

Cacas, M. C., E. Ledoux, G. de Marsily, B. Tillie, B. Barbreau, A. Durand, B. Feuga and P. Peaudecerf (1990), Modeling fracture flow with a stochastic discrete fracture network: Calibration and validation, 1, The flow model, *Water Resour. Res., 26*(3), pp. 479-489.

Caneiro, J. F. (2003), Probabilistic deliniation of groundwater protection zones in fractured-rock aquifers, Proceedings of the International conference on groundwater in fractured rocks, edited by J. Krasny, Z. Hrkal, and J. Bruthans, Prague, 15-19 Sept, 2003.

Cvetkovic, V., J. O. Selroos, and H. Cheng (1999), Transport of reactive tracers in rock fractures, *J. Fluid Mech*., *378*, pp. 335-356.

Cvetkovic, V., S. Painter, N. Outters, and J. O. Selroos (2004), Stochastic simulation of radionuclide migration in discretely fractured rock near the Äspö Hard Rock Laboratory, *Water Resour. Res*., *40*, W02404, doi:10.1029/2003WR002655.

Dagan, G. (1984), Solute transport in heterogeneous porous formations, *J. Fluid Mech*., *145*, 151-177.

Dershowitz, W, G. Lee, J. Geier, T. Foxford, P. LaPointe and A. Thomas (1998), *FracMan Interactive Discrete Feature Data Analysis, Geometric Modeling and Exploration Simulation*, User Documentation, Golder Associates Inc., Seattle, Washington.

Deutsch, C. V. and A. G. Journel (1998), *Geostatistical Software Library and User's Guide*, 2nd edition, Oxford University Press.

Domenico, P. A. and F. W. Schwarz (1998), *Physical and Chemical Hydrogeology*, 2nd edition, John Wiley & Sons, Inc., New York, NY, p. 230.

Dverstorp, B. and J. Andersson (1989), Application of the discrete fracture network concept with field data: Possibilities of model calibration and validation, *Water Resour. Res., 25*(3), pp. 540-550.

Endo, H. K., J. C. S. Long, C. K. Wilson, and P. A. Witherspoon (1984), A model for investigating mechanical transport in fractured media, *Water Resour. Res.*, *20*(10), pp. 1390-1400.

Gelhar, L. W. and C. L. Axness (1983), Three-dimensional stochastic analysis of macrodispersion in aquifers, *Water Resour. Res.*, *19*(1), pp. 161-180.

Harrison J. P. and J. A. Hudson (2000), *Engineering Rock Mechanics: Part 2. Illustrative examples*, Pergamon, Elsevier Science Ltd., The Boulevard, Longford Lane, Kidlington, Oxford OX5 1 GB, UK.

Hoffman, J. D. (2001), *Numerical Methods for Engineers and Scientists*, Second Edition Revised and Expanded, Marcel Dekker, Inc., New York, US.

Jackson, C. P., A. R. Hoch, and S. Todman (2000), Self-consistency of a heterogeneous continuum porous medium representation of fractured media. *Water Resour. Res*., *36*(1), pp. 189-202.

Käss, W. (1998), *Tracing Technique in Geohydrology*, A. A. Balkema, Rotterdam, Neatherlands, p 376.

Kosakowski, G. (2004), Anomalous transport of colloids and solutes in a shear zone, *J. Contam., Hydrol*., *72*, pp. 23-46.

Long, J. C. S., J. S. Remer, C. R. Wilson and P. A. Witherspoon (1982), Porous Media Equivalents for Networks of Discontinuous Fractures, *Water Resour. Res., 18*(3), pp. 645-658.

Miller, I., G. Lee and W. Dershowitz (1999), *MAFIC Matrix/Fracture Interaction Code With Heat and Solute Transport* User Documentation, Version 1.6, Golder Associates Inc., Redmond, Washington, November 30.

Moreno, L. and C.-F. Tsang (1994), Flow channeling in strongly heterogeneous porous media: A nummerical study, *Water Resour. Res*., *30*(5), pp. 1421-1430.

Neretnieks, I. (1993), Transport and Radionuclide Waste, in *Flow and contaminant transport in fractured rock*, edited by J. Bear, C.-F. Tsang and G. de Marsily, Academic Press, Inc., pp. 39-127.

Neuman, S. P. (1987), Stochastic continuum representation of fractured rock permeability as an alternative to REV and fracture network concepts, in Proceedings of the 28th U.S. Symposium on Rock Mechanics, edited by I. W. Farmer, et al., pp. 533-561, A. A. Balkema, Brookfield, Vt.

NGI (1993), Geotechnical (CSFT) laboratory testing of BVG joint samples from boreholes RCF1 and RCF3, Norwegian Geotechnical Institute Report 931005-102/2.

Nirex (1997a), The lithological and discontinuity characteristics of the Borrowdale Volcanic Group at outcrop in the Craghouse Park and Latterbarrow areas, Nirex Report SA/97/029.

Nirex (1997b), Evaluation of heterogeneity and scaling of fractures in the Borrowdale Volcanic group in the Sellafield area. Nirex Report SA/97/028.

Nirex (1997c), Data summary sheets in support of gross geotechnical predictions. Nirex Report SA/97/052.

Nirex (1997d), Assessment of the in situ stress field at Sellafield. Nirex Report SA/97/003.

Nordqvist, W., Y. W. Tsang, C.-F. Tsang, B. Dverstorp and J. Andersson (1992), A variable Aperture Fracture Network Model for Flow and Transport in Fractured Rocks, *Water Resour. Res*., *28*(6), pp. 1703-1713.

NRC (1996), *Rock fractures and fluid flow: Contemporary understanding and applications*., National Research Council, Committee on Fracture Characterization and Fluid Flow, U.S. National Committee for Rock Mechanics, National Academy Press, Washington DC, U.S., pp. 356-358.

Öhman, J. and A. Niemi (2003), Upscaling of Fracture Hydraulics by Means of an Oriented Correlated Stochastic Continuum Model, *Water Resour. Res*., *39* (10), 1277, doi:10.1029/2002WR001776.

Öhman, J., A. Niemi and J. Antikainen (2003), DECOVALEX III - The THM Upscaling Bench Mark Test, Progress Report, 28 May 2003 (www.decovalex.com).

Öhman, J., A. Niemi, and C.-F. Tsang (2004), Probabilistic Estimation of Fracture Transmissivity from Wellbore Hydraulic Data Accounting for Depth-Dependent Anisotropic Rock Stress (submitted to *Int. J. Rock Mech. and Min. Sci.,* 2004).

Osnes, J. D., A. Winberg and J. Andersson (1988), Analysis of Well Test Data – Application of Probabilistic Models to Infer Hydraulic Properties of Fractures, Topical Report RSI-0338, RE/SPEC Inc., Rapid City, South Dakota.

Parney, R. and L. Smith (1995), Fluid velocity and path-length in fractured media, *Geophys. Res. Lett., 22*(11), pp. 1437-1440.

Pruess, K., C. Oldenburg and G. Moridis (1999), *TOUGH2 User's Guide*, Version 2.0, Earth Science Division, Lawrence Berkeley National Laboratory University of California, Berkeley, California 94720, US.

Scher, H., G. Margolin and B. Berkowitz (2002), Towards a unified framework for anomalous transport in heterogeneous media, *Chemical Physics, 284*, pp. 349-359.

Schwartz, F. W. and L. Smith (1988), A continuum approach for modeling mass transport in fractured media, *Water Resour. Res., 24*(8), pp. 1360-1372.

Shulan, X., A. Wörman and B. Dverstorp (2001), Heterogeneous matrix diffusion in Crystalline rock – implications for geosphere retardation of migrating radionuclides, *J. Contam., Hydrol*., *47*, pp. 365-378.

Shapiro, A. M. (2001), Effective matrix diffusion in kilometer-scale transport in fractured crystalline rock, *Water Resour. Res., 37*(3), pp. 507-522.

Sidle, C.R., B. Nilsson, M. Hansen, J. Fredericia (1998), Spatially varying hydraulic and solute transport characteristics of a fractured till determined by field tracer tests, Funen, Denmark, *Water Resour. Res*. *34*(10), pp. 2515-2527.

Tsang, C.-F. (1993), Tracer transport in fracture systems, in *Flow and contaminant transport in fractured rock*, edited by J. Bear, C.-F. Tsang and G. de Marsily, Academic Press, Inc. pp. 237-266.

Tsang, C.-F. and I. Neretnieks (1998), Flow channeling in heterogeneous fractured rocks, *Rev. Geophys.*, *36*(2), pp. 275-298.

Tsang, C.-F., O. Stephansson, F. Kautsky, and L. Jing (2003), An Overview of the DECOVALEX Project on Coupled THM Processes in Fractured Rock-Bentonite Systems, Proceedings of GeoProc 2003 International Conference on Coupled THMC Processes in Geosystems, Stockholm, pp. 3–13, Oct. 13-15, 2003.

Tsang, C.-F. and Y. W. Tsang (1987), Channel Model of Flow through Fractured Media, *Water Resour. Res*. *23*(3), pp. 467-479.